

# Terahertz control of nanotip photoemission

L. Wimmer<sup>†</sup>, G. Herink<sup>†</sup>, D. R. Solli, S. V. Yalunin, K. E. Echternkamp and C. Ropers<sup>★</sup>

**The active control of matter by strong electromagnetic fields is of growing importance, with applications all across the optical spectrum from the extreme-ultraviolet to the far-infrared. In recent years, phase-stable terahertz fields have shown tremendous potential for observing and manipulating elementary excitations in solids<sup>1–3</sup>. In the gas phase, on the other hand, driving free charges with terahertz transients provides insight into ultrafast ionization dynamics<sup>4,5</sup>. Developing such approaches for locally enhanced terahertz fields in nanostructures will create new means to govern electron currents on the nanoscale. Here, we use single-cycle terahertz transients to demonstrate extensive control over nanotip photoelectron emission. The terahertz near-field is shown to either enhance or suppress photocurrents, with the tip acting as an ultrafast rectifying diode<sup>6</sup>. We record phase-resolved sub-cycle dynamics and find spectral compression and expansion arising from electron propagation within the terahertz near-field. These interactions produce rich spectro-temporal features and offer unprecedented control over ultrashort free electron pulses for imaging and diffraction.**

Controlling electric charges with external fields is at the heart of modern information technology, with ultimate bandwidths limited by switching speeds in nanoscopic devices. The term light-wave electronics illustrates the anticipated application of optically field-driven processes to solids, starting from schemes initially developed for atoms and molecules<sup>7,8</sup>. In the terahertz range, strong tabletop sources have opened up the field of nonlinear terahertz optics and are enabling comprehensive control over electronic or structural dynamics, for example, in the manipulation of spin waves, the triggering of phase transitions, and the implementation of terahertz-driven scanning tunnelling microscopy<sup>1–3,9–11</sup>. Completely new degrees of freedom are added by employing the localization of optical fields within nanostructures<sup>12–15</sup>. Specifically, at metallic nanotips, photoelectron emission<sup>16–18</sup> with characteristic strong-field features is observed<sup>19–21</sup>, including carrier-envelope-phase sensitivity<sup>22,23</sup>, and sub-cycle electron acceleration at mid-infrared frequencies<sup>12</sup>. A phase-resolved sampling of such processes may be achieved by so-called streaking spectroscopy, a method commonly applied in attosecond science, in which transient fields translate temporal information, for example, instances of ionization, into photoelectron energy or other degrees of freedom<sup>24–26</sup>.

The application of streaking spectroscopy to metallic nanostructures has been theoretically studied in-depth, aiming primarily at the full temporal characterization of near-infrared plasmonic fields<sup>27–31</sup>. However, the prospects of transferring these concepts to the terahertz domain have not yet been investigated.

Here, we show that the enhancement of terahertz fields in nanostructures allows for far-reaching electron trajectory control, spanning from phase-resolved streaking governed by the momentary electric field to propagation-induced spectral

reshaping. Experimentally, we demonstrate the terahertz control of electron dynamics using dual-frequency excitation of a gold nanotip: near-infrared pulses (800 nm wavelength, 50-fs pulse duration) induce nonlinear photoelectron emission from the tip apex, which is gated and streaked by locally enhanced single-cycle terahertz fields produced in a light-induced air plasma<sup>32,33</sup>. The experiment is sketched in Fig. 1 and represents a nanoscopic solid-state version of a terahertz streaking device.

We have recorded photoelectron energy spectra as a function of the delay between the terahertz and near-infrared pulses. This set of measurements comprises a spectrogram, in which both the delay-dependent modulation of the photocurrent and the kinetic energy distribution resolve the action of the terahertz field on the photoelectrons. Figure 2 presents such spectrograms for a very sharp tip (10 nm apex radius, Fig. 2b inset) and two incident terahertz waveforms of opposite polarities (Fig. 2a).

For large negative delays, that is, a situation in which the 800 nm pulse precedes the terahertz pulse, the photoelectron energy is set by the bias voltage (here: 30 V), and is unaffected by the terahertz field (Fig. 2b,d, delays  $< -2$  ps). In the delay range of temporal overlap between the near-infrared and terahertz pulses, the entire kinetic energy distribution is shifted in-phase with a rectifying photocurrent modulation (compare Fig. 2d,e) of three orders of magnitude, from a more than tenfold enhancement to a 98% suppression. The delay-dependent photocurrent (Fig. 2e) represents a direct measure of the instantaneous terahertz near-field strengths. This response is caused by a terahertz-modulation of the metal workfunction (Schottky effect) and the opening of lower-order multiphoton channels, as previously observed for static bias voltages<sup>17</sup>. The effect adiabatically follows the local terahertz field because the near-infrared photoemission process is much faster in comparison, ultimately limited by the few-femtosecond dephasing time of the localized tip plasmon<sup>34</sup>.

Whereas kinetic energy and photocurrent are strongly linked, some deviations to the incident terahertz field (characterized by electro-optic sampling<sup>35</sup>; Fig. 2a) are found, in particular as a small phase shift around the pulse centre and some oscillation at later times. These can be attributed to antenna properties of the conical tip affecting the local field at the apex<sup>36,37</sup>, and the present streaking measurements provide direct access to this local field (Supplementary Information).

The fact that the energy spectrogram (Fig. 2b,d) follows the local terahertz field in-phase is in stark contrast to common implementations of streaking in diffraction-limited laser foci, including attosecond streaking<sup>24</sup> and terahertz schemes to characterize X-ray and extreme-ultraviolet pulses<sup>4,38</sup>. Under such conditions, the streaking field is spatially homogeneous. For example, photoelectrons from an atomic gas experience the entire evolution of the streaking field  $F(t)$  after the time of emission  $t_e$ , resulting in the electron momentum  $P_{\text{streak}}$  governed by

IV. Physikalisches Institut, University of Göttingen, 37077 Göttingen, Germany. <sup>†</sup>These authors contributed equally to this work.

<sup>\*</sup>e-mail: c.ropers@gwdg.de

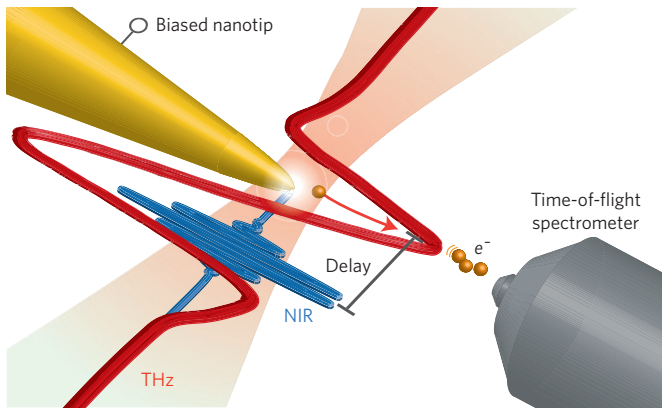


**Figure 1 | Control of nanotip photoemission with terahertz pulses.**

Ultrashort terahertz (red) and 800 nm near-infrared (NIR; blue) pulses are focused onto a metallic nanotip. The photoemission current and spectrum are recorded as a function of relative pulse delay.

the temporal integral over the field, that is, the vector potential  $A(t_e) : P_{\text{streak}} = eA(t_e) = e \int_{t_e}^{\infty} F(t') dt'$  (ref. 24). In contrast, for the very sharp tip used in Fig. 2, the nanolocalized streaking geometry allows electrons to escape the enhanced near-field within a small fraction of the terahertz oscillation period, yielding energies  $E_{\text{streak}}$  given by the instantaneous electrical potential<sup>27</sup>:  $E_{\text{streak}} \approx eU(t_e) = e \int F(r, t_e) dr$ . For a surface electric field decaying over a short length  $l_f$  and in the quasi-static limit, the energy gained is directly proportional to  $l_f eF(r = 0, t_e)$ . With decay lengths of only a few tens of nanometres and maximum energies of tens of electronvolts, local terahertz electric fields  $F \approx E_{\text{streak}}/el_f$  of multiple  $\text{MV cm}^{-1}$  are derived. As a result of the rectifying characteristic of this field emission geometry, the spectrograms exhibit gaps at times with strong electric force pointing towards the tip. To characterize the full temporal evolution of the terahertz near-field, we record two spectrograms using opposite polarities in the terahertz transient (Fig. 2b,d). Taking into account the respective polarities (Supplementary Information), these two complementary measurements can be superimposed to obtain—in analogy to attosecond streaking representations<sup>24</sup>—the smooth and continuous local terahertz electric waveform (Fig. 2d).

The extreme sub-cycle reduction of the interaction time with a localized driving field represents a limiting case of the recently observed quenching of the quiver motion at nanostructures<sup>12</sup>, and is phase-resolved here for the first time. The spatial adiabaticity parameter  $\delta = l_f m \omega^2 / eF$  relates the near-field decay length to an electron's quiver amplitude in an oscillating field and describes how closely the final energy follows the instantaneous electric field ( $\omega$ : excitation frequency,  $m$ : electron mass)<sup>12</sup>. Generally, the present conditions imply quasi-static acceleration, with  $\delta$ -values far below unity (for example,  $\delta = 0.01$  for  $F = 2 \text{ MV cm}^{-1}$ ,  $l_f = 10 \text{ nm}$  and at 1 THz frequency). However, close to the zero-crossings of the transient, a finite interaction time with the terahertz near-field becomes noticeable. At these delay times, where the photocurrent reappears after suppression ( $\tau = -0.5 \text{ ps}$  and  $+0.75 \text{ ps}$  in Fig. 2d), the onset of the spectrogram is slightly shifted above the bias voltage from electrons accumulating additional energy during propagation. While being almost negligible for the sharp tip used in the measurements of Fig. 2, such propagation effects become more pronounced with increasing tip radius, and in particular, will strongly depend on the initial velocity of photoemitted electrons traversing the near-field.

To investigate such more complex electron dynamics, we have carried out measurements using a tip with larger field decay length and a broader 'primary' photoemission spectrum induced

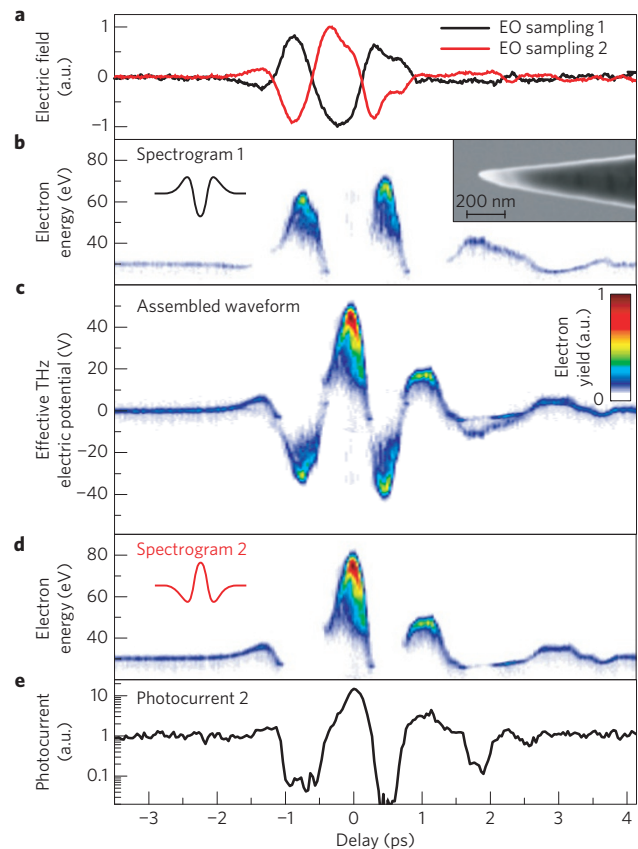


**Figure 2 | Terahertz-streaking spectroscopy of nanotip photoemission.**

- a**, Two terahertz transients with inverted field direction detected with electro-optic (EO) sampling at the measurement position of the tip.
- b**, Streaking spectrogram corresponding to EO trace 1. Inset: scanning electron micrograph of the nanotip used (radius: 10 nm).
- c**, Terahertz electric waveform derived from the measurements shown in **b,d** (see text).
- d**, Streaking spectrogram of the waveform corresponding to EO trace 2.
- e**, Photocurrent modulation from spectrogram 2 (shown in **d**).

by higher local near-infrared intensity. Figure 3 summarizes the results of this experiment, showing the delay-dependent modulation of the expectation value  $\langle E \rangle$  of the electron energy distributions and the high-energy cutoff (Fig. 3a), the photocurrent modulation (Fig. 3b) and the spectrogram (Fig. 3c). In the broader ensemble of initial energies generated by the near-infrared pulse alone (Fig. 3d), electrons probe the spatially and temporally varying field over different time intervals. Specifically, faster electrons rapidly sample the momentary terahertz field as they leave the apex region, while slower electrons experience integration over a time-varying transient. This has profound consequences in spectral redistributions, as evidenced by shape modulations in the spectrogram and the variation in the difference between  $\langle E \rangle$  and the high-energy cutoff. As a general result, we find substantial terahertz-induced spectral broadening and compression (Fig. 3e,f) as inherent features of propagation within a localized oscillating field. A temporally growing force causes spectral compression because initially slower electrons, which interact over a longer period with the rising terahertz field, experience more overall acceleration than initially faster electrons (compare sketch in Fig. 4f). Compression is apparent for various delays, for example, at  $-0.1 \text{ ps}$ ,  $+1.0 \text{ ps}$ ,  $+2.0 \text{ ps}$ . Spectral expansion, on the other hand, is a feature of a decreasing electric force: fast electrons leave the high field quasi-instantaneously, while slower electrons see a reduced potential, and are even decelerated as the force changes sign, see, for example, delays around  $-0.3 \text{ ps}$ ,  $+0.6 \text{ ps}$ ,  $+1.7 \text{ ps}$ . We note that these findings

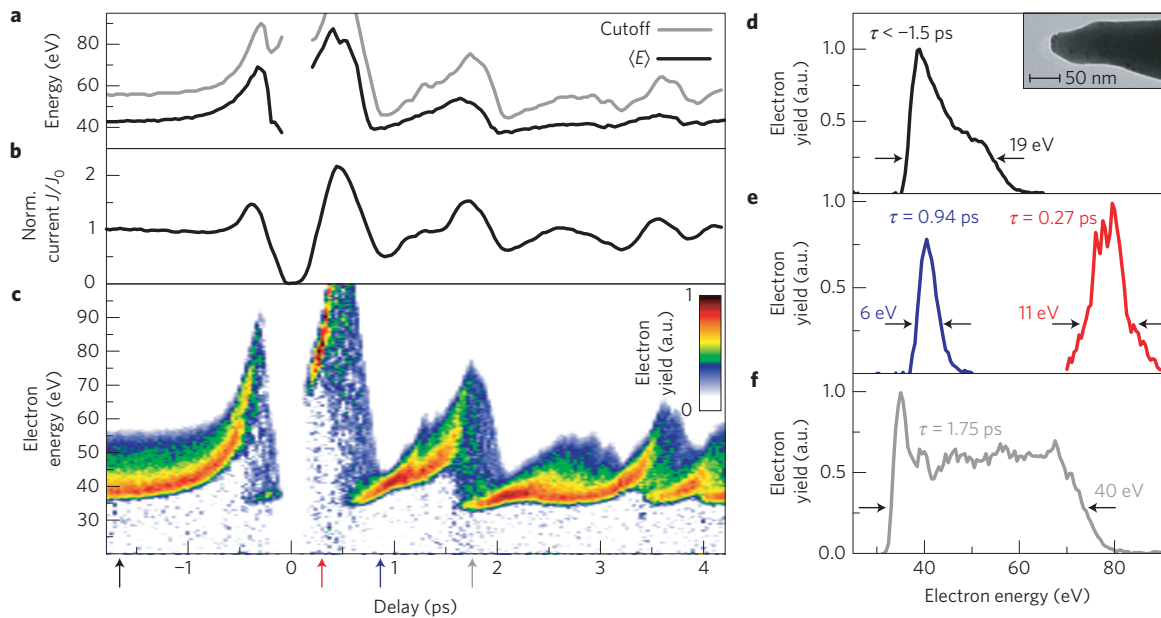


**Figure 3 | Spectral reshaping observed in streaking spectroscopy.** **a**, Expectation value of the energy distributions (black) and cutoff energy (grey) of the delay-dependent spectra. The high-energy cutoff is defined to include 95% of the electron distribution. **b**, Normalized photoemission current. **c**, Spectrogram. **d**, Energy spectrum unaffected by the terahertz pulse (large negative delay). Inset: transmission electron micrograph of the nanotip used. **e, f**, Individual spectra at selected delays showing terahertz-induced compression (blue), shifting (red) and expansion (grey). Coloured arrows in **c** indicate delay times of respective spectra (static bias:  $-40$  V).

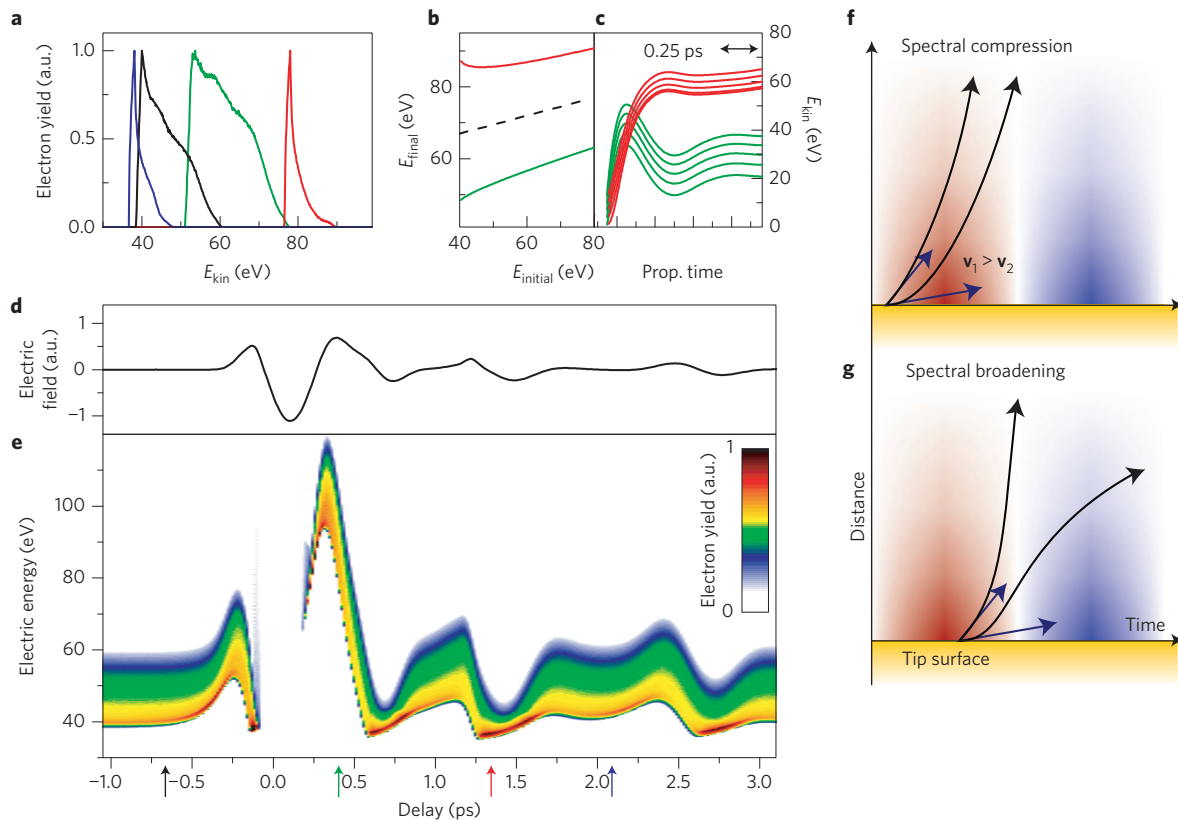


**Figure 4 | Simulation of terahertz streaking at a nanotip.** **a**, Energy spectra at different delay times. **b**, Final electron energy as a function of initial energy for two selected emission times corresponding to the spectra in **a**. Spectral compression (red) and broadening (green) are apparent (dashed line: unity slope for comparison). **c**, Temporal evolution of a set of five initial energies for these two emission times. Note that electrons have not yet acquired the full static potential within the plotted interval. **d**, Terahertz waveform as employed in the simulation. **e**, Simulated spectrogram. Colour-coded arrows indicate selected delays used in panels **a–c**. **f, g**, Illustrations of spectral compression (**f**) and broadening (**g**) for two different initial velocities ( $v_1, v_2$ ; blue arrows) induced by temporally rising and falling near-fields, respectively (red/blue: positive/negative force).



represent a nano-optical equivalent of radiofrequency spectral and temporal compression of ultrafast electron pulses, yet at orders of magnitude smaller temporal and spatial scales<sup>39</sup>.

Numerical modelling of the streaking spectrograms allows for a comprehensive description of the spatio-temporal acceleration process. Figure 4 presents results of a particle propagation simulation for a terahertz transient resembling that in Fig. 3. In the model, electron trajectories exposed to the locally enhanced terahertz field are computed for different emission times relative to the streaking transient, and for a distribution of initial velocities (Supplementary Information). Considering the different timescales involved, we can separate the effects on the electron spectra induced by the near-infrared photoemission field and by the terahertz streaking field: the near-infrared field causes the broadening of the initial kinetic energy spectrum by strong-field emission and acceleration<sup>12,19,20</sup>, as evident in the absence of the terahertz field at negative delays. In contrast, the terahertz field provides the shift and reshaping of the final spectra after emission. This approach is justified by the more than two orders of magnitude differing frequencies at which emission and streaking occur.

Figure 4a shows selected spectra simulated for various delay times, illustrating the strong spectral shaping induced by propagation in the spatially confined terahertz field (decay length 40 nm), see, for example, the spectral narrowing (blue, red) starting from the initially broader spectrum (black). The transfer function from initial to final energies for two selected emission times is plotted in Fig. 4b, while Fig. 4c shows the temporal evolution of a set of energies at two delay times resulting in spectral broadening (green) or compression (red). The full delay-dependent spectrogram (Fig. 4e) reproduces all main features of the measurements, including the terahertz-field-induced energy shift, current enhancement and suppression (Fig. 4d), as well as complex spectral reshaping. Even subtle characteristics, such as the narrow low-energy lobe at small negative delays, are successfully reproduced. The model computations allow us to quantitatively determine the magnitude of the local terahertz field. We obtain a peak field strength of  $9 \text{ MV cm}^{-1}$ , which amounts to a local field enhancement at the tip of about 90. At frequencies of only a few terahertz, such high fields are very hard to achieve in the absence of local field enhancements<sup>32,33,40</sup>, and are close to the threshold for terahertz-induced tunnelling<sup>11</sup> (Supplementary Information).

In conclusion, we demonstrate high-contrast switching and control of photocurrents and photoelectron spectra by tip-enhanced single-cycle terahertz pulses. In essence, the results represent the implementation of an ultrafast rectifying diode for the terahertz field, which is triggered by the near-infrared pulse. The spectral broadening and compression shown here amounts to a flexible tuning of the electron phase space density. The concept can be extended to other frequency ranges, provided that the involved spatial, temporal and energetic scales are suitably coupled along the particle trajectories. The approach has significant potential for the spectral and temporal optimization of electron pulses used in ultrafast electron diffraction and transmission electron microscopy, and may lead to a tailored focusing of electron pulses at controlled distances from the nanocathode.

Received 1 August 2013; accepted 15 April 2014;  
published online 25 May 2014

## References

- Schmittenmaier, C. A. Exploring dynamics in the far-infrared with terahertz spectroscopy. *Chem. Rev.* **104**, 1759–1780 (2004).
- Gaal, P. *et al.* Internal motions of a quasiparticle governing its ultrafast nonlinear response. *Nature* **450**, 1210–1213 (2007).
- Kampfrath, T., Tanaka, K. & Nelson, K. A. Resonant and nonresonant control over matter and light by intense terahertz transients. *Nature Photon.* **7**, 680–690 (2013).
- Frühling, U. *et al.* Single-shot terahertz-field-driven X-ray streak camera. *Nature Photon.* **3**, 523–528 (2009).
- Schütte, B., Frühling, U., Wieland, M., Azima, A. & Drescher, M. Electron wave packet sampling with laser-generated extreme ultraviolet and terahertz fields. *Opt. Express* **19**, 18833–18841 (2011).
- Evenson, K. M., Inguscio, M. & Jennings, D. A. Point contact diode at laser frequencies. *J. Appl. Phys.* **57**, 956–960 (1985).
- Goulielmakis, E. *et al.* Attosecond control and measurement: Lightwave electronics. *Science* **317**, 769–775 (2007).
- Schiffrin, A. *et al.* Optical-field-induced current in dielectrics. *Nature* **493**, 70–74 (2013).
- Fleischer, S., Zhou, Y., Field, R. W. & Nelson, K. A. Molecular orientation and alignment by intense single-cycle THz pulses. *Phys. Rev. Lett.* **107**, 163603 (2011).
- Liu, M. *et al.* Terahertz-field-induced insulator-to-metal transition in vanadium dioxide metamaterial. *Nature* **487**, 345–348 (2012).
- Cocker, T. L. *et al.* An ultrafast terahertz scanning tunnelling microscope. *Nature Photon.* **7**, 620–625 (2013).
- Herink, G., Solli, D. R., Gulde, M. & Ropers, C. Field-driven photoemission from nanostructures quenches the quiver motion. *Nature* **483**, 190–193 (2012).
- Ciappina, M. *et al.* Above-threshold ionization by few-cycle spatially inhomogeneous fields. *Phys. Rev. A* **86**, 023413 (2012).
- Yalunin, S. V. *et al.* Field localization and rescattering in tip-enhanced photoemission. *Ann. Phys. (Leipz.)* **525**, L12–L18 (2013).
- Sivis, M. & Ropers, C. Generation and bistability of a waveguide nanoplasma observed by enhanced extreme-ultraviolet fluorescence. *Phys. Rev. Lett.* **111**, 085001 (2013).
- Hommelhoff, P., Sortais, Y., Aghajani-Talesh, A. & Kasevich, M. A. Field emission tip as a nanometer source of free electron femtosecond pulses. *Phys. Rev. Lett.* **96**, 077401 (2006).
- Ropers, C., Solli, D. R., Schulz, C. P., Lienau, C. & Elsaesser, T. Localized multiphoton emission of femtosecond electron pulses from metal nanotips. *Phys. Rev. Lett.* **98**, 043907 (2007).
- Yanagisawa, H. *et al.* Energy distribution curves of ultrafast laser-induced field emission and their implications for electron dynamics. *Phys. Rev. Lett.* **107**, 087601 (2011).
- Bormann, R., Gulde, M., Weismann, A., Yalunin, S. V. & Ropers, C. Tip-enhanced strong-field photoemission. *Phys. Rev. Lett.* **105**, 147601 (2010).
- Schenk, M., Krüger, M. & Hommelhoff, P. Strong-field above-threshold photoemission from sharp metal tips. *Phys. Rev. Lett.* **105**, 257601 (2010).
- Park, D. J. *et al.* Strong field acceleration and steering of ultrafast electron pulses from a sharp metallic nanotip. *Phys. Rev. Lett.* **109**, 244803 (2012).
- Krüger, M., Schenk, M. & Hommelhoff, P. Attosecond control of electrons emitted from a nanoscale metal tip. *Nature* **475**, 78–81 (2011).
- Piglosiewicz, B. *et al.* Carrier-envelope phase effects on the strong-field photoemission of electrons from metallic nanostructures. *Nature Photon.* **8**, 37–42 (2014).
- Krausz, F. & Ivanov, M. Attosecond physics. *Rev. Mod. Phys.* **81**, 163–234 (2009).
- Kim, K. T. *et al.* Photonic streaking of attosecond pulse trains. *Nature Photon.* **7**, 651–656 (2013).
- Kirchner, F., Gliserin, A., Krausz, F. & Baum, P. Laser streaking of free electrons at 25 keV. *Nature Photon.* (2013).
- Stockman, M. I., Kling, M. F., Kleineberg, U. & Krausz, F. Attosecond nanoplasmonic-field microscope. *Nature Photon.* **1**, 539–544 (2007).
- Süßmann, F. & Kling, M. F. Attosecond nanoplasmonic streaking of localized fields near metal nanospheres. *Phys. Rev. B* **84**, 121406 (2011).
- Skopalová, E. *et al.* Numerical simulation of attosecond nanoplasmonic streaking. *New J. Phys.* **13**, 083003 (2011).
- Kelkensberg, F., Koenderink, A. & Vrakking, M. Attosecond streaking in a nano-plasmonic field. *New J. Phys.* **14**, 093034 (2012).
- Borisov, A. G., Echenique, P. M. & Kazansky, A. K. Attostreaking with metallic nano-objects. *New J. Phys.* **14**, 023036 (2012).
- Bartel, T., Gaal, P., Reimann, K., Woerner, M. & Elsaesser, T. Generation of single-cycle THz transients with high electric-field amplitudes. *Opt. Lett.* **30**, 2805–2807 (2005).
- Cook, D. J. & Hochstrasser, R. M. Intense terahertz pulses by four-wave rectification in air. *Opt. Lett.* **25**, 1210–1212 (2000).
- Anderson, A., Deryckx, K. S., Xu, X. G., Steinmeyer, G. & Raschke, M. B. Few-femtosecond plasmon dephasing of a single metallic nanostructure from optical response function reconstruction by interferometric frequency resolved optical gating. *Nano Lett.* **10**, 2519–2524 (2010).
- Schubert, O. *et al.* Ultrashort pulse characterization with a terahertz streak camera. *Opt. Lett.* **36**, 4458–4460 (2011).
- Wang, K., Mittleman, D. M., van der Valk, N. C. J. & Plancken, P. C. M. Antenna effects in terahertz apertureless near-field optical microscopy. *Appl. Phys. Lett.* **85**, 2715–2717 (2004).

37. Kersting, R., Chen, H.-T., Karpowicz, N. & Cho, G. C. Terahertz microscopy with submicrometre resolution. *J. Opt. A* **7**, S184–S189 (2005).
38. Grguras, *et al.* Ultrafast X-ray pulse characterization at free-electron lasers. *Nature Photon.* **6**, 852–857 (2012).
39. Oudheusden, T. v. *et al.* Compression of subrelativistic space-charge-dominated electron bunches for single-shot femtosecond electron diffraction. *Phys. Rev. Lett.* **105**, 264801 (2010).
40. Ulbricht, R., Hendry, E., Shan, J., Heinz, T. F. & Bonn, M. Carrier dynamics in semiconductors studied with time-resolved terahertz spectroscopy. *Rev. Mod. Phys.* **83**, 543–586 (2011).

### Acknowledgements

We thank K. Reimann, M. Wörner and T. Kampfrath for helpful discussions and B. Schröder, S. Schnell and A. Feist for technical support. We gratefully acknowledge financial support by the Deutsche Forschungsgemeinschaft (DFG-SPP 1391 'Ultrafast Nanooptics' and ZuK 45/1).

### Author contributions

L.W., G.H. and C.R. conceived and designed the experiment, which was set up by L.W., G.H., K.E.E. and D.R.S.. Experiments were carried out by L.W. and G.H., and the data were analysed by L.W., G.H. and C.R. The simulations were implemented by G.H., and an analytical model to determine simulation parameters was implemented by S.V.Y. All authors discussed the results and contributed to the interpretation, and the manuscript was written by L.W., G.H. and C.R.

### Additional information

Supplementary information is available in the [online version of the paper](#). Reprints and permissions information is available online at [www.nature.com/reprints](http://www.nature.com/reprints). Correspondence and requests for materials should be addressed to C.R.

### Competing financial interests

The authors declare no competing financial interests.